

# The mechanism of increased postnatal heart rate and sinoatrial node pacemaker activity in mice

Takeshi Adachi · Shigehiro Shibata ·  
Yosuke Okamoto · Shinichi Sato · Susumu Fujisawa ·  
Takayoshi Ohba · Kyoichi Ono

Received: 24 September 2012 / Accepted: 9 December 2012 / Published online: 4 January 2013  
© The Physiological Society of Japan and Springer Japan 2013

**Abstract** Heart rate (HR) of mammalian species changes postnatally, i.e., HR of large animals including humans decreases, while HR in small animals such as mice and rats increases. To clarify cellular mechanisms underlying the postnatal HR changes, we performed *in vivo* HR measurement and electrophysiological analysis on sinoatrial node (SAN) cells in mice. The *in vivo* HR was  $\sim 320$  beats  $\text{min}^{-1}$  (bpm) immediately after birth, and increased with age to  $\sim 690$  bpm at postnatal day 14. Under blockage of autonomic nervous systems, HR remained constant until postnatal day 5 and then increased day by day. The spontaneous beating rate of SAN preparation showed a similar postnatal change. The density of the L-type  $\text{Ca}^{2+}$  current (LCC) was smaller in neonatal SAN cells than in adult cells, accompanied by a positive shift of voltage-dependent activation. Thus, the postnatal increase in HR is caused by both the increased sympathetic influence and the intrinsic activity of SAN cells. The different conductance and kinetics of LCC may be involved in the postnatal increase in pacemaker activity.

**Keywords**  $\text{Ca}^{2+}$  current · Cardiac automaticity · Development · Hyperpolarization-activated cation channel · Heart rate · Sinoatrial node

## Introduction

It is well established that heart rate (HR) changes during the course of postnatal development in mammalian species. In general, the HR of large animals, including humans, rabbits [1, 2], and dogs [3], decreases with development. In humans, for example, HR is  $\sim 160$  beats  $\text{min}^{-1}$  (bpm) in neonates and  $\sim 60$  bpm in adults. By contrast, the HR of small animals such as mice [4] and rats [5] has been reported to increase after birth. These contrasting HR changes may be related to the size of the body and heart, and may be purposely designed to most effectively propel the blood to the body in various mammalian species. Nevertheless, the physiological significance and mechanisms underlying these postnatal changes in HR remain poorly understood. Two different mechanisms are likely involved in the postnatal change in HR. For example, it is well established that elevated vagal tone is involved in the slowing of HR in large animals [6]. Nevertheless, in newborn mice, it was reported that sympathetic control predominantly controlled basal HR, while there was negligible parasympathetic activity [4]. A change in the intrinsic spontaneous activity of sinoatrial node (SAN) cells is an alternative mechanism underlying developmental changes in HR. The spontaneous action potentials of sinoatrial pacemaker cells are produced by ion channels and transporters in SAN cells, as well as by intracellular  $\text{Ca}^{2+}$  dynamics [7, 8]. The expression and the resulting current density and/or the kinetics of ion channels is known to change during fetal and postnatal maturation, although the majority of studies utilized rabbit preparations in which the HR is expected to decrease during growth [2, 9–11]. In the present study, we examined the mechanisms of postnatal change in murine HR using *in vivo* non-invasive measurement of HR and

T. Adachi · S. Shibata · Y. Okamoto · S. Sato · S. Fujisawa ·  
T. Ohba · K. Ono (✉)  
Department of Cell Physiology,  
Akita University Graduate School of Medicine,  
1-1-1 Hondo, Akita 010-8543, Japan  
e-mail: onok@med.akita-u.ac.jp

electrophysiological analysis of ion channels in isolated SAN cells. Some of the results have been presented in preliminary form to the 89th annual meeting of the Physiological Society of Japan [12].

## Materials and methods

### Ethical approval

Animal care procedures were approved by the Animal Ethics Committee of Akita University Graduate School of Medicine, Japan.

### Measurement of heart rate in vivo

Non-invasive measurement of murine HR was accomplished using a piezoelectric transducer (PZT) sensor as described previously [4, 13]. In brief, C57BL/6J mouse pups aged 0–14 days born in our laboratory and adult mice aged 8–10 weeks were subjected to in vivo HR measurement. Both males and female pups were utilized. The PZT sensor was constructed simply by mounting a naked PZT (disk shaped, 35 mm outer diameter; EE35A-30A, FDK) on a copper plate (70 × 130 × 1 mm) with four small rubbers (2 mm thick) and then placing it on a heater-controlled PZT sensor, which was used as a heater device for temperature control. The PZT sensor output was amplified, connected to a handmade heart sound detector circuit, and stored in a computer by Clampex9 software with an analogue-to-digital converter (digidata1322A; Molecular Devices, Chicago, IL, USA) at a sampling interval of 200 μs. As previously described, temperature control is crucial for measuring HR, particularly in neonatal mice [4]. In the present study, the PZT surface temperature was set at 31 °C, and HR measurement was performed at a room temperature of 25 °C.

Mice at rest or sleep were placed onto the PZT sensor and underwent PZT recording for 5 min. Thereafter, atropine (2 mg kg<sup>-1</sup>) and metoprolol (2 mg kg<sup>-1</sup>) were administered intraperitoneally to mice using a 30-gauge insulin syringe (U-100; Becton–Dickinson) in order to eliminate the effects of sympathetic and parasympathetic contributions to the basal HR. Fifteen minutes later, PZT recording was performed for 5 min. HR was calculated by averaging 10 successive intervals of the first heart sound.

### SAN cell isolation

SAN cells were isolated from neonatal (P0–2) and adult wild-type mice. All adult mice were male. Mice were anaesthetized by intraperitoneal injection of pentobarbital sodium (120 μg g<sup>-1</sup>) including heparin (1,000 IU ml<sup>-1</sup>).

After retrograde injections of a Tyrode's and a Ca<sup>2+</sup>-free Tyrode's solution into the ascending aorta, the hearts were quickly removed and the SAN region was dissected in a normal Tyrode's solution at 35 °C. The SAN region was delimited by the borders of the crista terminalis, the interatrial septum, and the superior and inferior cava (see Fig. 1), as described previously [14, 15]. The SAN tissue was then treated in a Ca<sup>2+</sup>-free Tyrode's solution containing collagenase (Wako Pure Chemicals, Osaka, Japan) and elastase (Worthington, Lakewood, NJ, USA) for 30–60 min. After digestion, the tissue was rinsed in a high-K<sup>+</sup>, low-Cl<sup>-</sup> solution, and cells were dissociated by pipetting and stored in the same solution at 4 °C.

### Patch clamp experiments

A drop of cell suspension was added in the recording chamber (0.5 ml in volume) filled with normal Tyrode's solution. After the cells had settled on the floor of the recording chamber, they were perfused with normal Tyrode's solution at 2–3 ml min<sup>-1</sup>. SAN cells were visually identified by their characteristic morphology (spindle, elongated, or spider shape) and rhythmic spontaneous activity under the microscope. SAN cells were also identified electrophysiologically by their typical spontaneous action potentials with a slow diastolic depolarizing phase and by the existence of the hyperpolarization-activated current (*I<sub>f</sub>*) under whole-cell voltage-clamp recording. Cells that showed regular activity were used for the recording.

The whole-cell patch-clamp technique was used to record cellular automaticity and membrane currents with an Axopatch 200B (Molecular Devices) patch-clamp amplifier. Recording electrodes were fabricated from borosilicate glass capillaries with a microelectrode puller (P-97; Sutter instrument, Novato, CA, USA), and the tip resistance ranged from 2.5 to 4.5 MΩ when filled with internal solution. The liquid junction potential between the internal solution and the control Tyrode's solution was about -10 mV, so the recorded membrane potentials in the present study were corrected numerically. Spontaneous action potentials were recorded by the perforated patch-clamp technique with amphotericin B (0.2 mg ml<sup>-1</sup>). The membrane currents were recorded with the conventional whole-cell clamp condition. All electrophysiological experiments were performed at 35 ± 1 °C. Data acquisition was performed using the pClamp software (Molecular Devices). The sampling frequency was 10 kHz and low-pass filtering was performed at 2 kHz. The cell membrane capacitance (*C<sub>m</sub>*) was determined by applying a 30-ms hyperpolarizing voltage-clamp step from a holding potential of -50 to -60 mV and integrating the area under the capacitive transient. Analysis was performed with the Igor

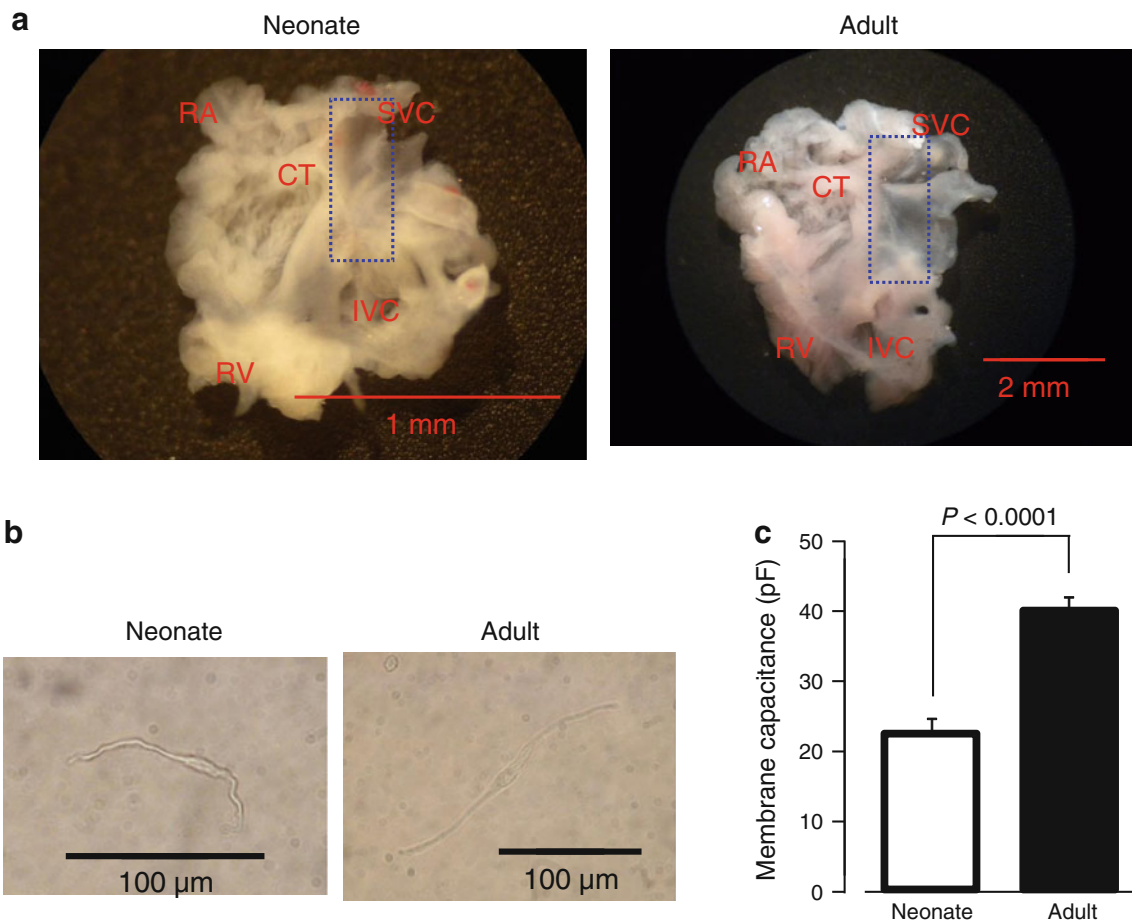


**Fig. 1** Isolated SAN preparation and cells from neonatal and adult mouse. **a** Photographs of whole SAN-atrial muscle preparations dissected from neonatal (*left*) and adult (*right*) mice. *CT* crista terminalis, *IVC* inferior vena cava, *RA* right auricle, *RV* right ventricle, *SVC* superior vena cava. The *dashed line* delimits the area

including SAN and the cutting edges used for intracellular potential recordings, SAN cells isolation, and qPCR. **b** Photographs of adult and newborn SAN cell. *Scale bar* 100 µm. **c** The membrane capacitance of SAN cells. Data are mean ± SEM

pro software (Wavemetrics, Portland, OR, USA) using macro-programs designed in-house.

### Intracellular potential recordings

Under deep anaesthesia with intraperitoneal injection of pentobarbital sodium (120 µg g<sup>-1</sup>) including heparin (1,000 IU ml<sup>-1</sup>), the heart was rapidly excised and atrial tissues containing the SAN area were dissected. The tissue preparation was then mounted in an organ bath and superfused with a standard external solution. The luminal side of the SAN area was impaled with glass microelectrodes filled with 3 M KCl to record transmembrane potential using a microelectrode amplifier (MEZ-8301; Nihon Kohden, Tokyo, Japan). Action potentials were displayed on an oscilloscope (2201; Tektronix, Beaverton, OR, USA), and were simultaneously recorded on a personal computer using

the LabChart software (AD Instruments, Colorado Springs, CO, USA).

### Solutions

The composition of the normal Tyrode’s solution (mM) was: NaCl 136.9, KCl 5.4, CaCl<sub>2</sub> 1.8, MgCl<sub>2</sub> 0.5, NaH<sub>2</sub>PO<sub>4</sub> 0.33, HEPES 5.0, and glucose 5.5 (pH 7.4 with NaOH). The high-K<sup>+</sup>, low-Cl<sup>-</sup> solution for cell storage contained (mM): L-glutamic acid 70, KOH 70, KCl 30, NaH<sub>2</sub>PO<sub>4</sub>, MgCl<sub>2</sub> 1, taurine 20, glucose 10, EGTA 0.3, and HEPES 10 (pH 7.4 with KOH). The standard external solution for the extracellular potential recordings contained (mM): NaCl 119, KCl 4.7, NaH<sub>2</sub>PO<sub>4</sub> 1.18, MgSO<sub>4</sub> 1.17, NaHCO<sub>3</sub> 25, glucose 5.5, CaCl<sub>2</sub> 1.8, atropine sulphate 0.005, and metoprolol tartrate 0.001, and was bubbled on oxygen and carbon dioxide. The external solution for recording

$I_f$  contained (in mM): NaCl 136.9, KCl 5.4,  $\text{NaH}_2\text{PO}_4$  0.33, HEPES 5, glucose 5.5,  $\text{MgCl}_2$  0.5,  $\text{CaCl}_2$  1.8, and  $\text{BaCl}_2$  2 (pH 7.4 with NaOH). The external solution for recording  $\text{Ca}^{2+}$  current was a  $\text{Na}^+$ ,  $\text{K}^+$ -free external solution that contained (mM): Tris-HCl 140,  $\text{CaCl}_2$  1.8,  $\text{MgCl}_2$  0.5, HEPES 5.0, and glucose 5.5 (pH 7.4 with Tris-base).

For perforation patch clamp recording, the pipette solution was composed of (mM): KOH 110, aspartic acid 110, KCl 30, NaCl 10, HEPES 5.0, and  $\text{CaCl}_2$  1.0 (pH 7.2 with KOH), with amphotericin B ( $0.2 \text{ mg ml}^{-1}$ ) added. The internal solution for extracellular potential recordings contained 3 M KCl. For recording  $\text{Ca}^{2+}$  currents, the internal solution contained (mM): CsOH 130, aspartic acid 80, TEA-Cl 20, Mg-ATP 5, EGTA 10, HEPES 5, and GTP-Tris<sub>2</sub> 0.1 (pH 7.2 with aspartic acid).

## Drugs

Chemicals and reagents were purchased from Sigma-Aldrich (St. Louis, MO, USA) or Wako Pure Chemicals, except for *N*-[4-[[1-[2-(6-methyl-2-pyridinyl)ethyl]-4-piperidinyl] carbonyl]phenyl] methanesulphonamide dihydrochloride (E4031) and 4-aminopyridine (4-AP). 4-AP was purchased from Nacalai Tesque (Kyoto, Japan). Stock solutions of atropine sulphate, metoprolol tartrate, E4031, 4-AP, TEA, and mibefradil were dissolved in the external solution to given concentrations described in the text, and used within a day.

## Quantitative real-time PCR

Quantitative PCR (qPCR) was used to measure the five transcripts ( $\text{Ca}_v1.2$ ,  $\text{Ca}_v1.3$ ,  $\text{Ca}_v3.1$ ,  $\text{Ca}_v3.2$ , and HCN4) in neonatal and adult mice. For qPCR, the SAN tissues collected from the right atrium were used as samples (the area enclosed by dashed lines shown in Fig. 1). RNA was extracted using ISOGEN II (Nippon Gene, Tokyo, Japan) following the manufacturer's protocol, and 1  $\mu\text{g}$  of total RNA was reverse transcribed. qPCR was performed using SYBR green technology. Experimental data were analyzed using the  $\Delta\Delta C_T$  method to obtain a quantitative measurement of mRNA abundance. The expression of each gene was normalized to that of glyceraldehyde-3-phosphate dehydrogenase (GAPDH).

## Data analysis and statistics

Results are expressed as mean  $\pm$  SEM. Statistical significance was evaluated using Student's *t* tests or one-way ANOVA followed by post hoc test with Bonferroni correction. A *P* value less than 0.05 was considered statistically significant. The number of experiments (*n*) is indicated in the figures or text.

## Results

### Postnatal change in the spontaneous activity of murine SAN

In order to characterize the postnatal changes of spontaneous activity in SAN cells, we first compared the HR of intact mice with the beating rates of SAN tissue preparation and isolated SAN cells at various postnatal ages. In the experiment shown in the Fig. 2a, a non-invasive measurement of HR was performed using the PZT sensor [4, 13]. Mice were simply placed on the PZT sensor, and the heart sound signal was extracted and used for calculating HR. HR was  $323 \pm 17 \text{ bpm}$  ( $n = 5$ ) at P0, and increased daily during 2 weeks after birth. The HR at P14 was  $685 \pm 18 \text{ bpm}$  ( $n = 5$ ), which was not significantly different from that in adult mice ( $703 \pm 12 \text{ bpm}$ ,  $n = 8$ ). These data are quantitatively similar to those reported previously [16]. Under pharmacological blockade of the autonomic nervous system with atropine and metoprolol, the HR of approximately 300 bpm was largely constant at P0–5, and then increased daily to 500 bpm at P14.

We next measured the spontaneous activity of SAN tissue preparation with the conventional microelectrode method. It should be noted that the intracellular recording of the action potential was not always successful in this experiment, particularly for the SAN preparation of newborn mice because the preparation was too small. As such, we did not analyze the action potential parameters such as amplitude, duration, and slow-diastolic depolarization. Instead, the beating rate could be evaluated even from the incomplete intracellular recording. The results were superimposed on the HR measurement of intact mice (Fig. 2a). The spontaneous beating rate was approximately 300 bpm immediately after birth and remained almost unchanged between P0 and P5, and then increased daily up to 400 bpm at P10. At P14, the beating rate of the SAN tissue preparation was  $441 \pm 14 \text{ bpm}$ . These findings indicate that the postnatal increase in HR is derived from increased sympathetic influence that becomes apparent immediately after birth, and increased intrinsic activity of SAN cells that emerges 5–6 days after birth.

To confirm the increase in the intrinsic activity of SAN cells, we recorded spontaneous action potentials in isolated SAN cells of neonatal (P0–1) and adult mice by the whole cell patch clamp method. Isolated SAN cells were morphologically similar between neonatal and adult mice (Fig. 1b; see also “Materials and methods”). The cell size, evaluated by measuring the membrane capacitance, was larger in SAN cells of adult mice than those of neonatal mice ( $39.8 \pm 2.1 \text{ pF}$ ,  $n = 36$  and  $22.3 \pm 2.1 \text{ pF}$ ,  $n = 25$  for adult and neonatal SAN cells, respectively). The action potentials recorded from isolated SAN cells are shown in

**Fig. 2** Developmental changes in SAN pacemaking activity. **a** Time course of changes in in vivo HR with (filled triangles) or without pharmacological blockade of autonomic nervous systems (filled squares) and spontaneous beating rate of SAN preparations (open circles) during postnatal development. Body weight is also shown in the lower graph. Number of experiments is indicated near each data. **b** Representative sweeps of spontaneous action potentials recorded in SAN cells of neonatal (left) and adult (right) mice. Data are mean  $\pm$  SEM

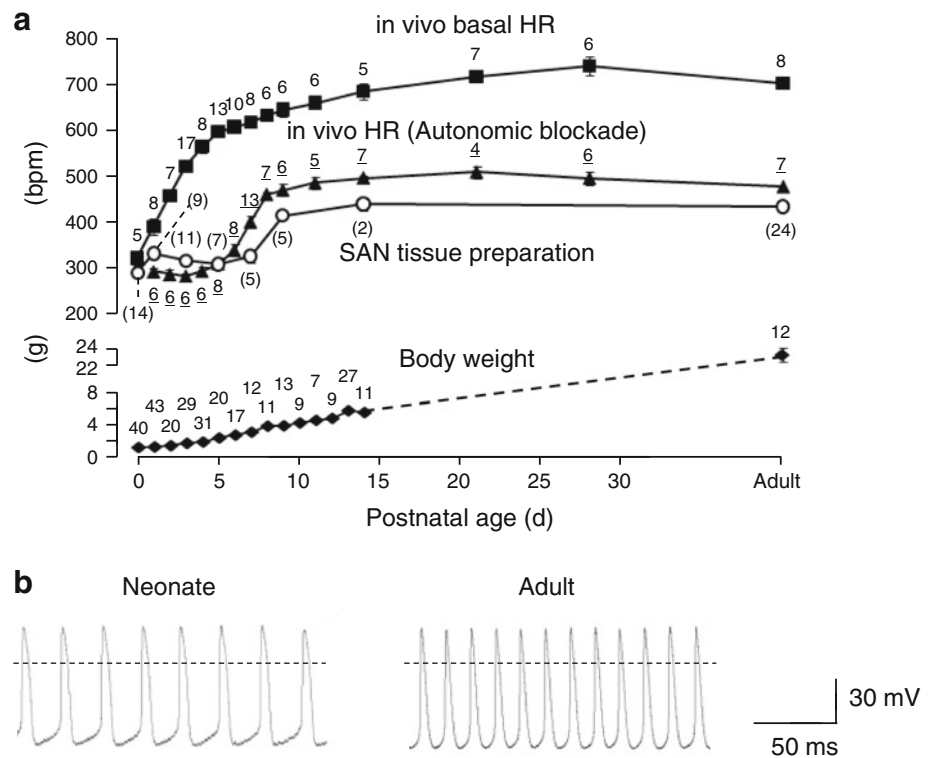


**Table 1** Comparison of spontaneous action potentials

Parameters	Neonate	Adult	<i>P</i> value
Beating rate (beats min <sup>-1</sup> )	249 $\pm$ 10	358 $\pm$ 19	0.0004
Overshoot (mV)	18.6 $\pm$ 3.0	15.8 $\pm$ 6.2	0.66
Maximal diastolic potential (mV)	-64.9 $\pm$ 3.0	-58.8 $\pm$ 2.4	0.19
Amplitude (mV)	83.5 $\pm$ 4.3	74.6 $\pm$ 7.9	0.31
Maximal upstroke velocity (V s <sup>-1</sup> )	14.9 $\pm$ 3.3	21.5 $\pm$ 5.6	0.31
50 % duration (mV)	51.3 $\pm$ 6.4	35.1 $\pm$ 2.9	0.089
Diastolic depolarization rate (mV s <sup>-1</sup> )	86 $\pm$ 7	180 $\pm$ 20	0.0008

Fig. 2b. The slow diastolic depolarization that is typical for SAN cells were evident in both neonatal (left) and adult (right) mice. The action potential parameters, which were obtained from six neonatal cells and four adult cells, were measured in 30 successive action potentials (Table 1). The beating rate and diastolic depolarization rate of SAN cells was significantly less in neonatal mice (249  $\pm$  10 bpm and 86  $\pm$  7 mV s<sup>-1</sup>, respectively) than in adult mice (358  $\pm$  19 bpm and 180  $\pm$  20 mV s<sup>-1</sup>, respectively). There were no differences in other parameters such as the overshoot, maximum diastolic potential, amplitude, maximal upstroke velocity, and 50 % duration between neonatal and adult pacemaker cells.

Pharmacological experiments

To explore the ionic nature of the increased intrinsic activity of SAN cells, we examined the pharmacological effects of various ion channel inhibitors on the spontaneous beating rate of SAN tissue preparations (Fig. 3). Application of 2 mM Cs<sup>+</sup>, an inhibitor for I<sub>f</sub>, reduced the firing frequency of SAN tissues at all postnatal ages, although the extent of the reduction became less marked with postnatal age. On average, 2 mM Cs<sup>+</sup> reduced the firing frequency of SAN tissues by 39.0  $\pm$  2.0 % (n = 13), 32.3  $\pm$  1.4 % (n = 15), 19.7  $\pm$  2.3 % (n = 5), and 19.2  $\pm$  2.7 % (n = 10) in P0–3, P5–7, P10, and adult mice, respectively. By contrast, 10  $\mu$ M mibefradil, which inhibits both I<sub>CaT</sub> and I<sub>CaL</sub>, reduced the firing frequency of SAN preparation by 11.1  $\pm$  0.9 % (n = 5) in adult mice, but by only 3.2  $\pm$  1.0 % (n = 4) in neonatal mice (P < 0.001). There were no differences in spontaneous activity of SAN tissues between neonate and adult mice using 50  $\mu$ M Ni<sup>2+</sup>, 5  $\mu$ M E4031, 5 mM 4-AP, and 20 mM TEA), although all these substances, more or less, reduced the firing frequency (Fig. 3).

Whole cell current of SAN cells in neonatal and adult mice

The representative whole cell currents recorded from isolated SAN cells of neonatal and adult mice are shown in

**Fig. 3** Pharmacology of the SAN pacemaker activity during the postnatal development. **a–f** Percentage inhibition of pacemaking activity by 2 mM  $\text{Cs}^+$ , 50  $\mu\text{M}$   $\text{Ni}^{2+}$ , 10  $\mu\text{M}$  mibefradil, 5  $\mu\text{M}$  E4031, 1 mM 4-AP, and 25 mM TEA in neonatal and adult SAN preparations. Note that the inhibition by  $\text{Cs}^+$  is more marked in neonatal than in adult mice, and that the inhibition of mibefradil is more marked in adult than in neonate mice. Numbers of experiments are indicated in parentheses. Data are mean  $\pm$  SEM

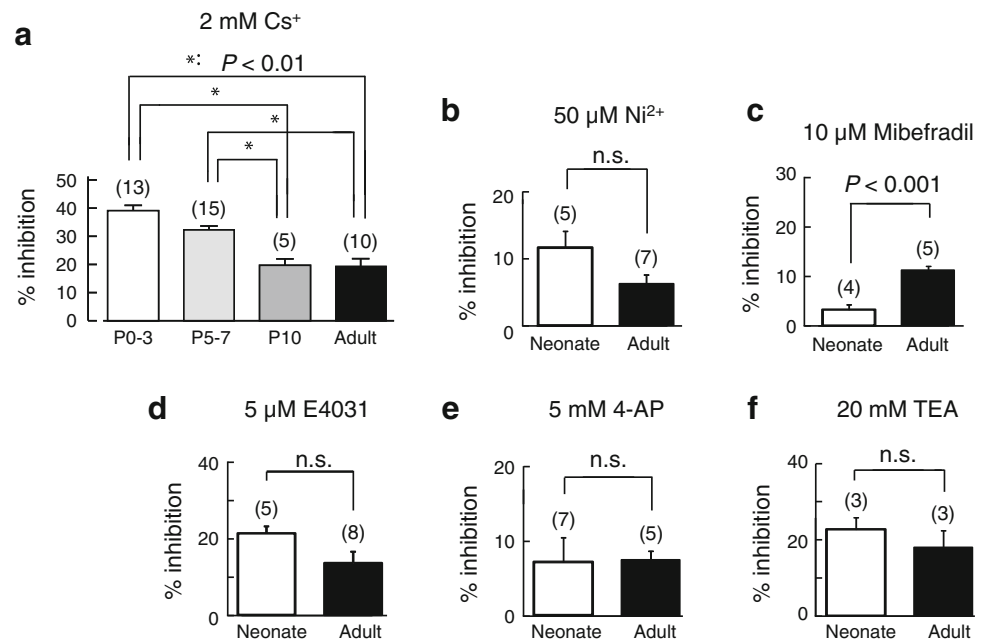


**Fig. 4.** Under the voltage clamp condition, the membrane potential was held at  $-50$  mV and the test pulses of 500-ms duration were applied to various potentials from  $-140$  to  $+50$  mV in 10-mV increments. Depolarizing pulses also induced activation of the calcium current followed by time-dependent outward currents. Hyperpolarizing pulses produced a slow and continuous increase of the inward current,  $I_f$ . The current–voltage ( $I$ – $V$ ) relationships, shown in circles indicating initial peak currents and boxes indicating end currents, are illustrated in Fig. 4. Open and filled symbols display the currents obtained from neonatal and adult mice, respectively. The  $I$ – $V$  relationships were qualitatively similar between neonatal and adult SAN cells. In fact, no significant differences were detected in the current amplitude at the initial and end of test pulses between neonatal and adult SAN cells ( $n = 4$ , both neonate and adult).

#### $I_f$ in neonate and adult pacemaker cells

To further examine the ionic mechanisms underlying the postnatal increase in the firing frequency of SAN cells, we investigated the properties of  $I_f$ , an important pacemaker current, in SAN cells of neonate and adult mice.  $I_f$  was recorded under the blockage of the inward rectifier  $\text{K}^+$  current and the  $\text{Ca}^{2+}$  current using 1 mM  $\text{Ba}^{2+}$  and 1.8 mM  $\text{Ni}^{2+}$  substituted for  $\text{Ca}^{2+}$  in normal Tyrode's solution. Figure 5a shows families of representative current traces recorded in SAN cells of neonate and adult mice. Currents were obtained using 2-s hyperpolarizing pulses from the holding potential of  $-50$  mV to various potentials

in 10-mV steps. The amplitude of the currents, measured at the beginning and end of the pulses, were normalized in reference to the cell capacitance and plotted against the test potentials (Fig. 5b). No significant difference was detected in the  $I_f$  density between neonatal and adult SAN cells. The quasi-steady state activation of  $I_f$  was evaluated by measuring the amplitude of the tail current (the time-dependent current,  $I_{td}$ ). The  $I_{td}$  amplitude was normalized to the maximal value of  $I_{td}$  ( $I_{td-max}$ ). The relationship between the test potentials ( $V_m$ ) and the  $I_{td}$  amplitude was fitted with the Boltzmann equation:

$$I_{td}/I_{td-max} = 100/[1 + \exp\{(V_m - V_{0.5})/S\}]$$

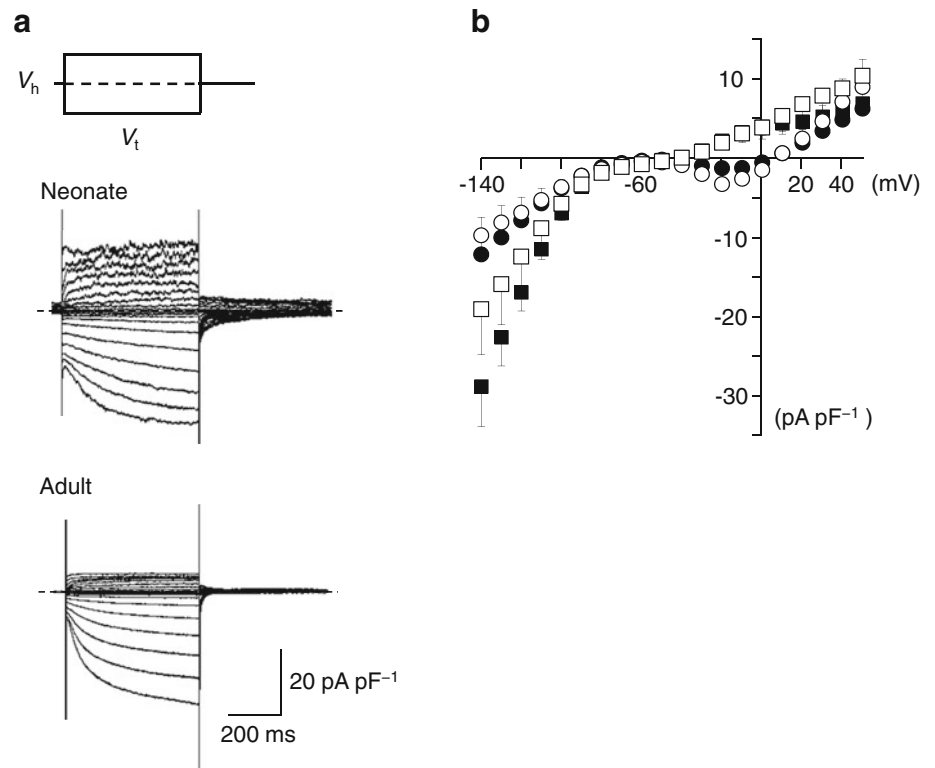
where  $V_{0.5}$  is the membrane potential for the half-maximal activation and  $S$  is the slope factor (Fig. 5c). The values for  $V_{0.5}$  and  $S$ , determined by a least-squares fit, were  $-100.5 \pm 4.7$  mV and  $9.8 \pm 1.4$  ( $n = 6$ ), respectively, in SAN cells from neonate mice, and  $-103.9 \pm 3.7$  mV and  $11.4 \pm 1.6$  ( $n = 5$ ), respectively, in cells from adult mice. There were no significant differences in  $V_{0.5}$  and  $S$  between neonatal and adult SAN cells ( $P = 0.602$  for  $V_{0.5}$  and  $P = 0.478$  for  $S$ ).

#### L- and T-type channel $\text{Ca}^{2+}$ current in neonate and adult pacemaker cells

Next, we analyzed the L- ( $I_{CaL}$ ) and T-type  $\text{Ca}^{2+}$  currents ( $I_{CaT}$ ) (Fig. 6). To suppress voltage-dependent  $\text{Na}^+$  current and various  $\text{K}^+$  currents, the pipette solution and the bath solution were  $\text{Na}^+$ - and  $\text{K}^+$ -free. Under the whole-cell condition, the membrane potential was held at  $-60$  mV

**Fig. 4** Membrane currents and current–voltage relationships of isolated single SAN cells from neonatal and adult mice.

**a** Whole-cell current of a SAN cell of neonatal (*upper traces*) and adult mice (*lower traces*) in normal Tyrode’s solution. Traces shown were obtained by applying 500-ms depolarizing or hyperpolarizing pulses from a holding potential ( $V_h$ ) of  $-50$  mV in 10-mV increments. *Dashed lines* indicate the zero current level. **b** Current–voltage relationships for the initial current (*open circles* neonate, *filled circles* adult) and the current near the end of the pulses (*open squares* neonate, *filled squares* adult). Data are mean  $\pm$  SEM



and 300-ms depolarizing pulses were applied to various potentials in 10-mV steps to record  $I_{CaL}$ . Representative current recordings obtained from SAN cells of neonatal and adult mice are shown in Fig. 6a.  $I_{CaL}$  was activated at potentials more positive than  $-50$  mV, peaking at  $-10$  mV, in SAN cells from adult mice. These findings agree with previous studies [15, 17–22]. By contrast,  $I_{CaL}$  was activated at more positive potentials in SAN cells from neonatal mice; i.e., the threshold potential was approximately  $-30$  mV with a peak at  $+10$  mV. Figure 6b showed the  $I$ – $V$  relationships obtained from six experiments in adult mice and five experiments in neonatal mice. In order to quantitatively analyze the voltage dependence of  $I_{CaL}$  activation, the peak  $I_{CaL}$  amplitude was measured, and the chord conductance was calculated by dividing the  $I_{CaL}$  amplitude at various test potentials ( $V_t$ ) by the driving force,  $V_t - E_{rev}$ .  $E_{rev}$  is the reversal potential, which was assumed approximately  $+50$  mV from the  $I$ – $V$  curve in Fig. 6b. The obtained curves were fitted with a single Boltzmann function,

$$G/G_{max} = 1/[1 + \exp\{(V_{0.5} - V)/S\}]$$

where  $G/G_{max}$  indicates the relative chord conductance. The voltage for half-inactivation ( $V_{0.5}$ ) and  $S$  were  $-9.1 \pm 3.0$  mV and  $13.3 \pm 2.7$  ( $n = 5$ ), respectively, in neonatal cells and  $-28.4 \pm 5.4$  mV and  $9.7 \pm 1.0$  ( $n = 6$ ), respectively, in adult SAN cells ( $P = 0.015$  and  $P = 0.20$ ) (Fig. 6c). These findings confirmed that the  $I_{CaL}$

activation was shifted to more positive voltages in neonatal SAN cells compared with adult cells (Fig. 6b).

The steady-state inactivation was analysed by a double-pulse protocol; 7-s conditioning prepulses to different potentials were followed by the test pulse to 0 mV. The amplitude of  $I_{CaL}$  was measured, normalized to the maximal value of  $I_{CaL}$  ( $I_{CaL-max}$ ), and fitted with Boltzmann equation:

$$I_{CaL}/I_{CaL-max} = 1/[1 + \exp\{(V_m - V_{0.5})/S\}]$$

The values of  $V_{0.5}$  and  $S$  were  $-43.0 \pm 1.5$  mV and  $8.0 \pm 0.5$  ( $n = 6$ ), respectively, in neonatal cells and  $-41.5 \pm 2.4$  mV and  $7.4 \pm 0.5$  ( $n = 10$ ), respectively, in adult SAN cells ( $P = 0.66$  and  $P = 0.45$ ) (Fig. 6c).

The  $I_{CaT}$  was analyzed as a low-voltage-activated  $Ca^{2+}$  current. As shown in Fig. 7a, the current traces obtained with 300-ms test pulses to  $-50$  mV from holding potentials of  $-100$  and  $-60$  mV indicates the existence of a low-voltage-activated  $Ca^{2+}$  current,  $I_{CaT}$ . Representative traces of  $I_{CaT}$  at various test potentials ranging from  $-90$  to  $+50$  mV, defined as the difference current, are shown in Fig. 7b, indicating that  $I_{CaT}$  exists both in neonatal and adult SAN cells. The  $I$ – $V$  relationships for  $I_{CaT}$ , obtained from five cells are shown in Fig. 7c, where the initial peak (open circles, neonate; filled circles, adult) and the current near the end of the pulses (open squares, neonate; filled squares, adult) are plotted against the test potentials. Although the  $I_{CaT}$  amplitude seemed smaller in neonatal

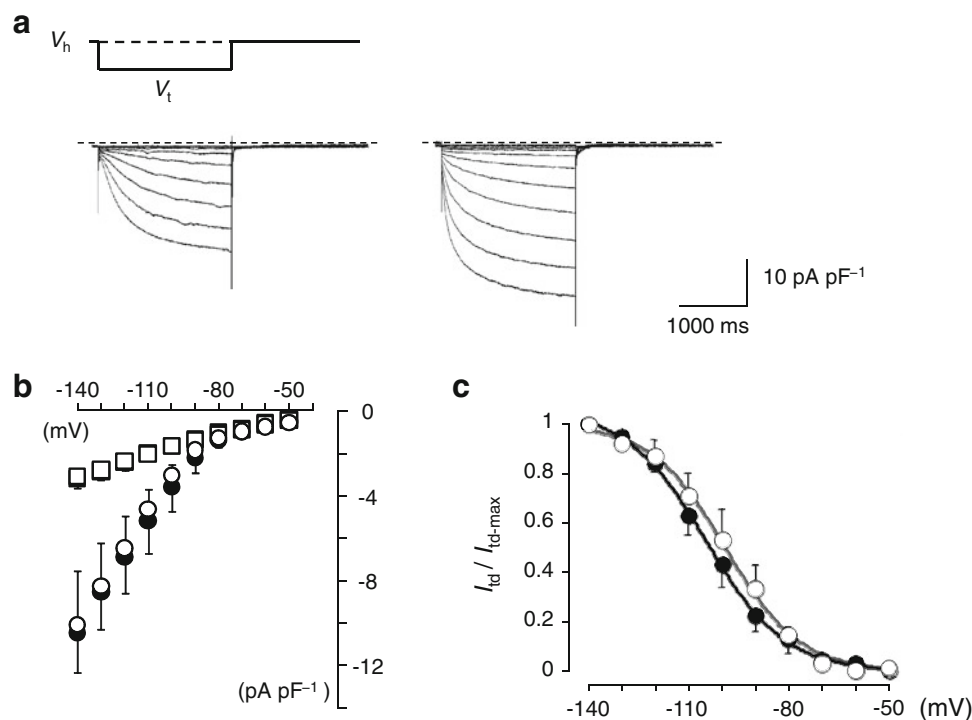


**Fig. 5**  $I_f$  in isolated SAN cells from neonatal and adult mice. **a** Whole-cell current of neonatal (*left*) and adult (*right*) SAN cell in external solution containing 1.8 mM  $\text{Ni}^{2+}$  and 1 mM  $\text{Ba}^{2+}$ . The holding potential ( $V_h$ ) was  $-50$  mV and 2-s depolarizing pulses were applied in 10-mV increments.  $V_t$ , test potential. **b** Current–voltage relationships for the initial current (*squares*) and the current at the end of the 2-s pulses (*circles*). *Open* and *filled* symbols indicate neonatal

and adult mice, respectively. Data are means of six and five cells for neonatal and adult SAN cells, respectively. **c** Voltage-dependent activation of  $I_f$ . The tail current amplitude was normalized in reference to that of the maximal amplitude and plotted against the membrane potential. The smooth curves were drawn by the least squares fit with the Boltzmann equation. Data are mean  $\pm$  SEM

SAN cells than in adult cells, we failed to obtain statistical significance in the  $I_{\text{CaT}}$  density between neonatal and adult SAN cells. The steady-state inactivation was analysed using a double-pulse protocol. The magnitude of the  $I_{\text{CaT}}$  was normalized to the maximal value of  $I_{\text{CaT}}$  ( $I_{\text{CaT-max}}$ ), and the relationship of inactivation  $I_{\text{CaT}}$  was fitted with the Boltzmann equation:

$$I_{\text{CaT}}/I_{\text{CaT-max}} = 1/[1 + \exp\{(V_m - V_{0.5})/S\}]$$

The peak  $I_{\text{CaT}}$  density,  $V_{0.5}$ , and  $S$  were  $-2.4 \pm 0.5$  pA pF $^{-1}$ ,  $-74.4 \pm 2.2$ , and  $4.1 \pm 0.6$  ( $n = 6$ ), respectively, in adult SAN cells. The peak  $I_{\text{CaT}}$  density was  $-1.4 \pm 0.3$  pA pF $^{-1}$  in neonatal SAN cells, which was not different than adult SAN cells ( $P = 0.17$ ). The values of  $V_{0.5}$  and  $S$  were  $-72.1 \pm 0.5$  mV and  $1.8 \pm 0.4$  ( $n = 5$ ), respectively. The relatively steeper slope was likely due to a low signal/noise ratio in some experiments. When the least squares fit with the Boltzmann equation was applied with a constant slope factor of 4.0, the  $V_{0.5}$  was  $-72.6 \pm 1.3$  mV in neonatal SAN cells. We consider that the conductance and the kinetics of  $I_{\text{CaT}}$  were not different between neonatal and adult SAN cells.

Gene expression of  $\text{Ca}_v1.2$ ,  $\text{Ca}_v1.3$ ,  $\text{Ca}_v3.1$ ,  $\text{Ca}_v3.2$ , and HCN4 in neonatal and adult SAN tissue

To examine whether the mRNA expression of cloned  $\text{Ca}^{2+}$  channels and HCN4 channels are involved in the postnatal change of pacemaker activity, we performed qPCR using the SAN tissue preparations obtained from neonatal (P0–2) and adult mice. We investigated the level of gene expression for  $\text{Ca}_v1.2$ ,  $\text{Ca}_v1.3$ ,  $\text{Ca}_v3.1$ ,  $\text{Ca}_v3.2$ , and HCN4, which are known to encode ion channels responsible for  $I_{\text{CaL}}$  ( $\text{Ca}_v1.2$ ,  $\text{Ca}_v1.3$ ),  $I_{\text{CaT}}$  ( $\text{Ca}_v3.1$ ,  $\text{Ca}_v3.2$ ), and  $I_f$  (HCN4) (Fig. 8). There were no statistical differences in the expression levels of  $\text{Ca}_v1.2$ ,  $\text{Ca}_v1.3$ ,  $\text{Ca}_v3.1$ ,  $\text{Ca}_v3.2$ , and HCN4 between neonate and adult SAN tissues.

## Discussion

Although the HR of mammalian species is known to change during the course of postnatal development, quantitative measurement of HR and the intrinsic pacemaker activity of SAN have not been systematically

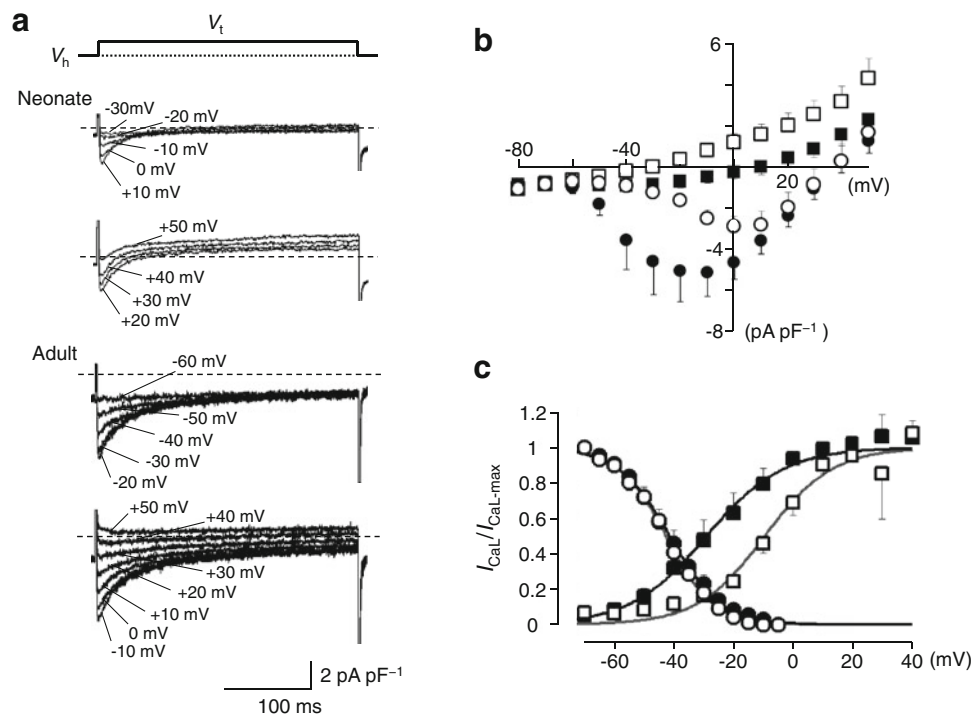


**Fig. 6**  $I_{CaL}$  in isolated SAN cells from neonatal and adult mice. **a** Representative traces of  $I_{CaL}$  in SAN cells from neonatal (upper panel) and adult mice (lower panel). Traces shown were obtained by applying 300-ms depolarizing voltage pulses from a holding potential ( $V_h$ ) of  $-60$  mV to variable voltages ( $V_t$ ) indicated. The pipette solution was a  $Cs^+$ -rich solution and the external solution was  $Na^+$  and  $K^+$ -free. Dotted lines indicate the zero current level. **b** Averaged current–voltage relationships for the initial current (circles) and the current at the end of the 500-ms pulses (squares). Open and filled symbols indicate neonatal and adult mice, respectively. **c** Voltage-

dependent activation and inactivation for  $I_{CaL}$  in SAN cells from neonatal and adult mice. The steady-state inactivation was analysed by a double-pulse protocol; 7-s conditioning prepulses to different potentials were followed by the test pulse to 0 mV. The amplitude of  $I_{CaL}$  was measured, normalized to the maximal value of  $I_{CaL}$  and fitted with Boltzmann equation. Open and filled symbols indicate neonatal and adult mice, respectively. Voltage-dependent activation was obtained by calculating the chord conductance of peak  $I_{CaL}$  at various test potentials in SAN cells from neonatal (open squares) and adult (filled squares) mice. Data are mean  $\pm$  SEM

performed, particularly in small animals. In this study, we performed in vivo HR measurement and electrophysiological analysis on SAN preparation and isolated SAN cells at various postnatal stages in mice. The in vivo HR was measured using the PZT sensor, which enabled non-invasive measurement of HR even in neonatal mice [4, 13], with little interference from anaesthetics and stressor stimuli. This is particularly important as the HR of neonatal mice is easily influenced by various stressor stimuli. Isolation of murine SAN cell is also technically difficult owing to the small size of the dominant pacemaker region in the mouse heart [14]. Despite the extremely small size of the neonatal mouse heart, isolated pacemaker cells possessed similar morphological and electrophysiological characteristics for sinoatrial pacemaker cells to those previously reported [7, 18]. The in vivo basal HR was approximately 320 bpm at P0, and increased with age to  $\sim$ 690 bpm at P14. Under the pharmacological blockage of autonomic nervous systems, HR was  $\sim$ 300 bpm at P0 and remained constant until P5, and then increased with age to  $\sim$ 450 bpm at P14. The spontaneous beating rate of the

SAN preparation showed a similar ontogenetic change with that observed in in vivo study, and isolated SAN cells demonstrated spontaneous activities with a frequency that increased with postnatal age. Thus, we consider that the postnatal change of the murine HR was successfully quantified in the present study. Further, our data indicate that the postnatal increase in the basal HR is caused by increased sympathetic influence that becomes apparent immediately after birth, and by intrinsic activity of SAN cells that emerges 5–6 days after birth.

#### Developmental change in HR and influence of autonomic nervous system

Autonomic control of pacemaker activity in vivo is based on concomitant input from sympathetic and parasympathetic nerves. However, the ratio between vagal and sympathetic input varies depending on various mammalian species. Large animals such as dogs and humans are under prominent vagal tone, as pharmacological block of the autonomic input significantly accelerates the basal HR

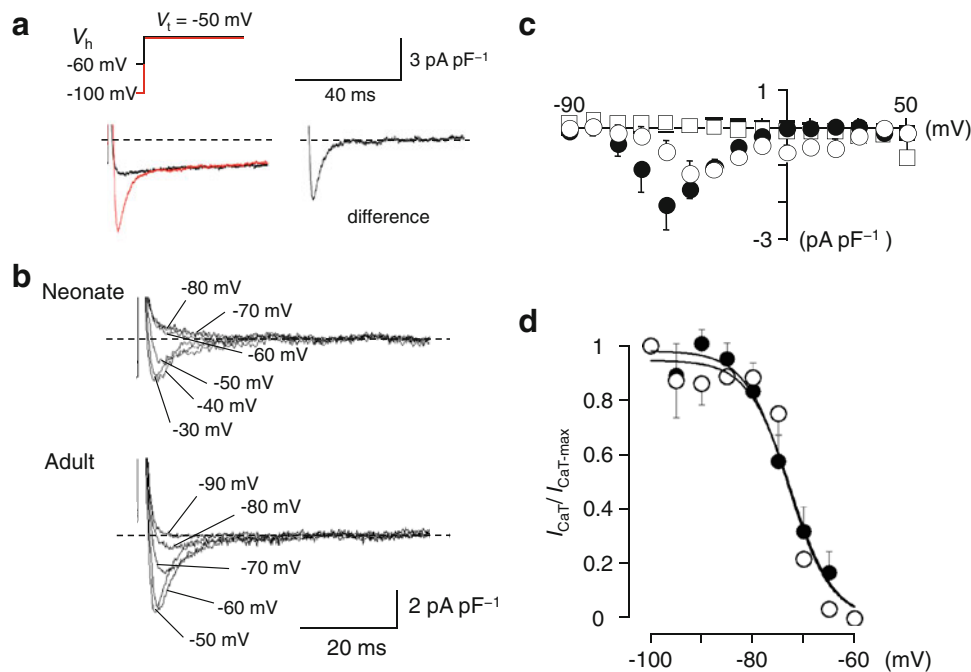


**Fig. 7**  $I_{CaT}$  in isolated SAN cells from neonatal and adult mice. **a** Representative traces showing the isolation of  $I_{CaT}$ . Superimposed current traces recorded by 300-ms depolarizing pulses from a holding potential of  $-100$  and  $-60$  mV in adult SAN cells. The difference current is shown in the *right panel*. **b** Superimposed current traces were difference currents at various test potentials obtained from neonatal (*upper traces*) and adult (*lower traces*) by the pulse protocols shown in (**a**). *Dotted lines* indicate the zero current level.

**c** Averaged current–voltage relationships of  $I_{CaT}$  in pacemaker cells for the initial current (*circles*) and the current at the end of the 500-ms pulses (*squares*). *Open and filled symbols* indicate neonatal and adult mice, respectively. **d** Steady-state inactivation curves for  $I_{CaT}$  in SAN cells from neonatal (*open circles*) and adult (*filled circles*) mice. The smooth curves were drawn by the least squares fit with the Boltzmann equation. Data are mean  $\pm$  SEM

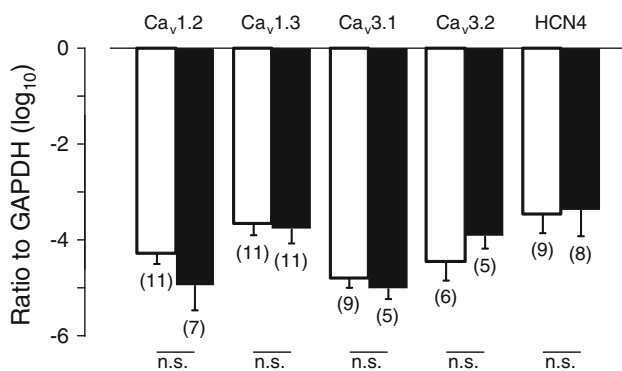


**Fig. 8** Comparison of  $Ca_v1.2$ ,  $Ca_v1.3$ ,  $Ca_v3.1$ ,  $Ca_v3.2$ , and HCN4 expression in SAN tissues from neonatal and adult mice. mRNA expression of  $Ca_v1.2$ ,  $Ca_v1.3$ ,  $Ca_v3.1$ ,  $Ca_v3.2$ , and HCN4 in neonatal and adult mouse SAN cells were measured using qPCR. The expression of each gene was normalized to that of GAPDH. *Open and filled columns* correspond to neonatal and adult mice, respectively. Numbers of experiments are indicated in *parentheses*. Data are mean  $\pm$  SEM

[23]. By contrast, the basal HR of mice is likely to be greatly elevated by tonic adrenergic stimulation irrespective of various postnatal stages. In fact, pharmacological blockage of autonomic nervous systems decreased the

*in vivo* HR throughout postnatal development (Fig. 2; as previously reported in adult mice [24]). In addition, using tyrosine hydroxylase immunohistochemistry, sympathetic nerve endings were reported to appear at embryonic day 15, and were apparent in the myocardium at P1 and P42 [25], while tyrosine hydroxylase-positive nerves were most abundant in the SAN in the heart [25]. By contrast, the influence of the parasympathetic nervous system on basal HR is negligible in mice, particularly in neonates. It was previously reported that parasympathetic blockade with atropine had no effect on basal HR in neonatal mice, and a transient bradycardia response to attachment of electrocardiographic electrodes developed between P4 and P8, which was attributed to phasic vagal efferent activation [4]. Further, cholinergic innervation into the SAN was reported to develop postnatally in mice; i.e., the majority of the SAN lacked cholinergic innervation immediately after birth, and showed a notable increase at  $\sim$ P7.5 [26].

Postnatal changes in the spontaneous action potential and possible candidates of ionic channels and/or ion transporters that underlie the pacemaker mechanism have been typically investigated using rabbit preparations, which show postnatal slowing, not increase, in the HR [2, 9–11, 27]. Toda [27] demonstrated that the spontaneous beating

rate of rabbit SANs decreased during postnatal development, accompanied by prolongation of the action potential duration and an increasingly negative maximal diastolic potential. Recording of ionic currents by the patch clamp method revealed an  $\sim 35\%$  decrease in the  $I_f$  density [9], a reduction in the  $\text{Na}^+$  current ( $I_{\text{Na}}$ ) [28], and a decrease in  $I_{\text{CaL}}$  density [29]. Further, Allah et al. [30] reported a significant postnatal decrease in HCN4,  $\text{Na}_v1.5$ ,  $\text{Ca}_v1.3$ , and NCX1 mRNAs, responsible for major inward currents ( $I_f$ ,  $I_{\text{Na}}$ ,  $I_{\text{CaL}}$ , and  $\text{Na}^+/\text{Ca}^{2+}$  exchange current, respectively), and significant postnatal decrease in the delayed rectifier  $\text{K}^+$  channels ( $\text{K}_v1.5$ , ERG,  $\text{K}_v\text{LQT1}$ , and minK). These electrophysiological and molecular data apparently favor the postnatal slowing of intrinsic HR, but cannot be extended to small animals such as mice and rats.

Ionic mechanisms underlying the postnatal increase in the spontaneous activity of mouse SAN cells

The action potentials of SAN cells of neonatal mice showed essentially similar configurations when compared with adult SAN cells, except for a slower diastolic depolarization. Whole-cell voltage-clamped experiments demonstrated that SAN cells in both neonatal and adult mice possessed major inward and outward currents reported previously. Among them,  $I_f$  is known to play a key role in the pacemaker depolarization in the SAN and is a key determinant of HR [31]. The molecular determinants for  $I_f$  were identified as HCN channels that comprise four isoforms, and the major component of the native SAN  $I_f$  is generally the HCN4 isoform in rabbits [32, 33] and in mice [34–36]. In the present study, we failed to detect differences in the current density, the kinetics of  $I_f$ , and the expression of HCN4 mRNA between neonatal and adult SAN cells. The finding is obviously different from those reported in rabbit preparations, where the  $I_f$  current density was significantly larger in newborn SAN cells than in adult cells [9] or where the threshold potential of  $I_f$  shifted to more negative potentials in adult SAN cells [2]. The expression of HCN4 mRNA was also reported to be significantly less in adult SAN tissues than that in neonates in rabbits [30]. Thus, the contribution of  $I_f$  to postnatal changes in the intrinsic activity of SAN cells may be species-dependent.

It should be noted that the spontaneous beating rate was decreased by 2 mM  $\text{Cs}^+$  in the SAN tissue preparation, while the extent of this decrease was more marked in newborn than in adult mice. The finding cannot be explained if the increased intrinsic activity of mouse SAN during postnatal development was the result of an increased contribution of  $I_f$  to pacemaker activity. However, the finding may be explained if the current density and activation kinetics of  $I_f$  remained unchanged during

postnatal development, as the contribution of  $I_f$  is expected to become more marked in cells with a relatively slower beating rate [37]. Thus, the postnatal increase in the pacemaker activity of the SAN may be derived from ionic current systems other than  $I_f$  channels. We also consider that  $I_f$  plays a more significant role in pacemaker activity in neonatal SAN cells than in adults.

There was a marked difference in the voltage-dependent properties of  $I_{\text{CaL}}$  between newborn and adult SAN cells in the present study. The configurations of  $I_{\text{CaL}}$  in adult SAN cells are in good accordance with those reported in mouse SAN cells; i.e., the activation threshold was near  $-50$  mV with the peak amplitude at  $-10$  mV. On the other hand, the  $I_{\text{CaL}}$  appeared to be activated at more positive potentials and the current amplitude was smaller in newborn SAN cells than in adult cells (Fig. 6). It was reported that the  $\text{Ca}^{2+}$  channels of SAN cells are derived from  $\text{Ca}_v1.2$  and  $\text{Ca}_v1.3$ , and that recombinant and native  $\text{Ca}_v1.3$ -mediated  $I_{\text{CaL}}$  displayed a more negative activation threshold than  $\text{Ca}_v1.2$ -mediated  $I_{\text{CaL}}$ . Further, Mangoni et al. [15] reported that  $I_{\text{CaL}}$   $I$ - $V$  relationships in SAN cells from  $\text{Ca}_v1.3^{-/-}$  mice exhibited current activation shifted to more positive voltages by 22 mV when compared with wild-type SAN cells. Thus, it might be speculated that  $I_{\text{CaL}}$  in newborn mice SAN cells were derived chiefly from  $\text{Ca}_v1.2$ . However, this is unlikely as our qPCR experiment failed to detect significant differences in the expression of  $\text{Ca}_v1.2$  and  $\text{Ca}_v1.3$  mRNA levels. Nevertheless, alternative splicing has been identified as an important regulator of voltage-dependent  $\text{Ca}^{2+}$  channels. Singh et al. [38] found that alternative splicing in the  $\text{Ca}_v1.3$  subunit C terminus expressed  $I_{\text{CaL}}$ , which was activated at more depolarized potentials. Haase et al. [39] also reported that expression of the rat cardiac 250-kDa  $\text{Ca}_v1.2$  subunit increased approximately 10-fold from fetal days 12–20 and declined during postnatal maturation, while the 220-kDa  $\text{Ca}_v1.2$  decreased to undetectable levels. Thus, it is possible that splice variants of  $\text{Ca}_v1.2$  and/or  $\text{Ca}_v1.3$ , which were not identified in the present study, may account for the different voltage-dependent property and current density between newborn and adult SAN cells in mice. Alternatively, intrinsic channel properties may change during development owing to the modulation of  $\text{Ca}^{2+}$  channels. In the SAN,  $I_{\text{CaL}}$  is regulated by protein kinase A and by activated  $\text{Ca}^{2+}$ /calmodulin-dependent protein kinase II, which regulates the current activation and reactivation kinetics [7]. It was reported that the basal level of global cAMP in SAN cells exceeds that in ventricular myocytes, mediating robust basal protein kinase A-dependent phosphorylation of specific surface membrane ion channels and  $\text{Ca}^{2+}$  cycling proteins, which regulates the periodicity and amplitude of spontaneous activity of SAN cells [8]. Yang et al. [2] reported that basal cAMP production is reduced during the

postnatal development in rabbit SAN cells, contributing to the slowing of HR after birth in this animal species. In this respect, it is interesting to know whether the basal cAMP production increases after birth in mice, in parallel to the postnatal increase in HR and the negative shift of the  $I_{CaL}$  activation. Further studies are necessary to elucidate the cellular mechanisms of kinetic change in  $I_{CaL}$ . Nevertheless, differences in the properties of  $I_{CaL}$  may contribute, at least in part, to the postnatal increase of the mouse HR.

$I_{CaT}$  was recorded as a low-voltage activated  $Ca^{2+}$  current, and we failed to detect significant changes in the current density and kinetic properties between newborn and adult SAN cells. Further, the expression levels of  $Ca_v3.1$  and  $Ca_v3.2$  were not different. These findings are in good agreement with a previous study reporting no differences in  $I_{CaT}$  in newborn and adult rabbit SAN cells [29]. The lack of differences in the inhibition of spontaneous activity by  $Ni^{2+}$  between neonates and adults (Fig. 3) in our study supports this view. On the other hand, mibefradil inhibited the spontaneous activity more strongly in adults than in neonates at a concentration of 10  $\mu M$  (Fig. 3). We speculate that the pronounced inhibition of the spontaneous activity in adult SAN cells is likely due to inhibition of both  $I_{CaT}$  and  $I_{CaL}$ . It is well known that T-type  $Ca^{2+}$  channels in SAN are derived from  $Ca_v3.1$  and  $Ca_v3.2$  [40–43], and that  $Ni^{2+}$  is more sensitive to  $Ca_v3.2$  than  $Ca_v3.1$  [44, 46], whereas mibefradil inhibited both isoforms of T-type channels and  $I_{CaL}$  [45–47]. Of note, however, the amplitude of  $I_{CaT}$  varied from cell to cell in the present study, which might have caused underestimation of the  $I_{CaT}$  contribution to the postnatal increase in the beating rate of SAN cells.

#### Potential limitations

Although we addressed the cellular mechanisms underlying the postnatal increase in the spontaneous activity of mouse SAN cells, there are a number of limitations that should be resolved in future experiments. Firstly, it was quite difficult to excise the sinoatrial region because the area is so small, particularly in neonatal mice (see Fig. 1). It is thus possible that the differences of the mRNA expression level between neonates SAN cells and adult SAN cells might have been masked by genes obtained from contaminating atrial cells. Secondly, the spontaneous activity of single SAN cells was recorded only in neonatal and adult mice, and no information about the time course of the increase in the beating rate of SAN cells was given in the present study. Thus, it is not yet decided whether the increased beating rate in SAN tissue preparation is derived entirely from the increased activity of SAN cells, or different mechanisms are embedded in the tissue level. Thirdly, we analyzed only  $I_f$ ,  $I_{CaL}$ , and  $I_{CaT}$  in the present study, and the roles of other

ionic current systems including  $I_{Na}$ , sustained inward current,  $Na^+-Ca^{2+}$  exchange current,  $Na^+-K^+$  pump current, delayed rectifier  $K^+$  currents, inward rectifier  $K^+$  current, transient outward current,  $Cl^-$  current, and non-selective inward current [7] remain unresolved. For example, a significant contribution of TTX-sensitive and TTX-resistant components of  $I_{Na}$  to the control of spontaneous rate of isolated SAN cells [48] has been demonstrated. Further, the current density of TTX-sensitive  $I_{Na}$  was markedly greater in SAN cells from newborn canines, but decreased with age [11]. It remains unclear whether other currents vary developmentally. Finally, we have not addressed possible contribution of intracellular  $Ca^{2+}$  to postnatal increase in SAN pacemaker activity. Intracellular  $Ca^{2+}$  release is an important mechanism for promoting automaticity at rest, and for acceleration of the HR under sympathetic nerve input [8]. The  $Ca^{2+}$  stores in cardiac cells during embryogenesis and postnatal development exhibit considerable diversity in the release channels and regional differences in  $Ca^{2+}$  signalling [49]. Thus, it is feasible that the relative contribution of the  $Ca^{2+}$  clock to SAN spontaneous action potentials may also change during postnatal development. Future studies are required to examine the developmental changes in SAN automaticity in relation to the activity of ion channels and intracellular  $Ca^{2+}$  dynamics.

#### Conclusion

We provide the first successful recordings of in vivo HR and action potentials of isolated SAN cells at various postnatal stages of mice. As the mouse model is extensively used in genetic studies of mammalian development, it is important to consider the difference in developmental changes in basal HR and cardiac autonomic regulation of HR in the heart between mice and other large animals including humans. The present study provides a comprehensive functional study of spontaneous action potentials and ionic currents during postnatal development in the mouse.

**Acknowledgment** This study was supported by Grants-in-Aid from the Ministry of Education, Culture, Sports, Science and Technology of Japan to K.O. (#22500363, #23136501).

#### References

1. Hewett KW, Rosen MR (1985) Developmental changes in the rabbit sinus node action potential and its response to adrenergic agonists. *J Pharmacol Exp Ther* 235:308–312
2. Yang ZF, Sun Y, Li CZ, Wang HW, Wang XJ, Zheng YQ, Liu K, Liu YM (2006) Reduced sinoatrial cAMP content plays a role in postnatal heart rate slowing in the rabbit. *Clin Exp Pharmacol Physiol* 33:757–762

3. Woods WT, Urthaler F, James TN (1978) Progressive postnatal changes in sinus node response to atropine and propranolol. *Am J Physiol* 234:412–415
4. Sato S (2008) Quantitative evaluation of ontogenetic change in heart rate and its autonomic regulation in newborn mice with the use of a noninvasive piezoelectric sensor. *Am J Physiol Heart Circ Physiol* 294:1708–1715
5. Tucker DC (1985) Components of functional sympathetic control of heart rate in neonatal rats. *Am J Physiol* 248:601–610
6. Chow LT, Chow SS, Anderson RH, Gosling JA (2001) Autonomic innervation of the human cardiac conduction system: changes from infancy to senility—an immunohistochemical and histochemical analysis. *Anat Rec* 264:169–182
7. Mangoni ME, Nargeot J (2008) Genesis and regulation of the heart automaticity. *Physiol Rev* 88:919–982
8. Lakatta EG, Maltsev VA, Vinogradova TM (2010) A coupled SYSTEM of intracellular  $Ca^{2+}$  clocks and surface membrane voltage clocks controls the timekeeping mechanism of the heart's pacemaker. *Circ Res* 106:659–673
9. Accilli EA, Robinson RB, DiFrancesco D (1997) Properties and modulation of  $I_f$  in newborn versus adult cardiac SA node. *Am J Physiol* 272:1549–1552
10. Baruscotti M, Robinson RB (2007) Electrophysiology and pacemaker function of the developing sinoatrial node. *Am J Physiol Heart Circ Physiol* 293:2613–2623
11. Protas L, Oren RV, Clancy CE, Robinson RB (2010) Age-dependent changes in Na current magnitude and TTX-sensitivity in the canine sinoatrial node. *J Mol Cell Cardiol* 48:172–180
12. Adachi T, Okamoto Y, Sato S, Fujisawa S, Ohba T, Shibata S, Ono K (2012) Postnatal change of pacemaker activity in murine sino-atrial node. *J Physiol Sci* 62(suppl 1):2PJ–120
13. Sato S, Yamada K, Inagaki N (2006) System for simultaneously monitoring heart and breathing rate in mice using a piezoelectric transducer. *Med Biol Eng Comput* 44:353–362
14. Verheijck EE, van Kempen MJ, Veereschild M, Lurvink J, Jongasma HJ, Bouman LN (2001) Electrophysiological features of the mouse sinoatrial node in relation to connexin distribution. *Cardiovasc Res* 52:40–50
15. Mangoni ME, Couette B, Bourinet E, Platzer J, Reimer D (2003) Functional role of L-type  $Ca_v1.3$   $Ca^{2+}$  channels in cardiac pacemaker activity. *Proc Natl Acad Sci USA* 100:5543–5548
16. Heier CR, Hampton TG, Wang D, Didonato CJ (2010) Development of electrocardiogram intervals during growth of FVB/N neonate mice. *BMC Physiol* 24:10–16
17. Mangoni ME, Traboulsie A, Leoni AL, Couette B, Marger L, Le Quang K, Kupfer E, Cohen-Solal A, Vilar J, Shin HS, Escande D, Charpentier F, Nargeot J, Lory P (2006) Bradycardia and slowing of the atrioventricular conduction in mice lacking  $Ca_v1.3$  T-type calcium channels. *Circ Res* 98:1422–1430
18. Cho HS, Takano M, Noma A (2003) The electrophysiological properties of spontaneously beating pacemaker cells isolated from mouse sinoatrial node. *J Physiol* 550:169–180
19. Rose RA, Kabir MG, Backx PH (2007) Altered heart rate and sinoatrial node function in mice lacking the cAMP regulator phosphoinositide 3-kinase-gamma. *Circ Res* 101:1274–1282
20. Rose RA, Sellan M, Simpson JA, Izaddoustdar F, Cifelli C, Panama BK, Davis M, Zhao D, Markhani M, Murphy GG, Striessnig J, Liu PP, Heximer SP, Backx PH (2011) Iron overload decreases  $Ca_v1.3$ -dependent L-type  $Ca^{2+}$  currents leading to bradycardia, altered electrical conduction, and atrial fibrillation. *Circ Arrhythm Electrophysiol* 4:733–742
21. Springer J, Azer J, Hua R, Robbins C, Adamczyk A, McBoyle S, Bissell MB, Rose RA (2012) The natriuretic peptides BNP and CNP increase heart rate and electrical conduction by stimulating ionic currents in the sinoatrial node and atrial myocardium following activation of guanylyl cyclase-linked natriuretic peptide receptors. *J Mol Cell Cardiol* 52:1122–1134
22. Hua R, Adamczyk A, Robbins C, Ray G, Rose RA (2012) Distinct patterns of constitutive phosphodiesterase activity in mouse sinoatrial node and atrial myocardium. *PLoS One* 7:1–12
23. Ophhof T (2000) The normal range and determinants of the intrinsic heart rate in man. *Cardiovasc Res* 45:177–184
24. Gehrmann J, Hammer PE, Maguire CT, Wakimoto H, Triedman JK, Berul CI (2000) Phenotypic screening for heart rate variability in the mouse. *Am J Physiol Heart Circ Physiol* 279:733–740
25. Jeda M, Kanazawa H, Kimura K, Hattori F, Ieda Y, Taniguchi M, Lee JK, Matsumura K, Tomita Y, Miyoshi S, Shimoda K, Makino S, Sano M, Kodama I, Ogawa S, Fukuda K (2007) Sema3a maintains normal heart rhythm through sympathetic innervation patterning. *Nat Med* 13:604–612
26. Fregoso SP, Hoover DB (2012) Development of cardiac parasympathetic neurons, glial cells, and regional cholinergic innervation of the mouse heart. *Neuroscience* 221:28–36
27. Toda N (1980) Age-related changes in the transmembrane potential of isolated rabbit sino-atrial nodes and atria. *Cardiovasc Res* 14:58–63
28. Baruscotti M, DiFrancesco D, Robinson RB (1996) A TTX-sensitive inward sodium current contributes to spontaneous activity in newborn rabbit sino-atrial node cells. *J Physiol* 492:21–30
29. Protas L, DiFrancesco D, Robinson RB (2001) L-type but not T-type calcium current changes during postnatal development in rabbit sinoatrial node. *Am J Physiol Heart Circ Physiol* 281:1252–1959
30. Allah EA, Tellez JO, Yanni J, Nelson T, Monfredi O, Boyett MR, Dobrzynski H (2011) Changes in the expression of ion channels, connexins and  $Ca^{2+}$ -handling proteins in the sino-atrial node during postnatal development. *Exp Physiol* 96:426–438
31. DiFrancesco D (2010) The role of the funny current in pacemaker activity. *Circ Res* 106:434–446
32. Ishii TM, Takano M, Xie LH, Noma A, Ohmori H (1999) Molecular characterization of the hyperpolarization-activated cation channel in rabbit heart sinoatrial node. *J Biol Chem* 274:12835–12839
33. Shi W, Wymore R, Yu H, Wu J, Wymore RT, Pan Z, Robinson RB, Dixon JE, McKinnon D, Cohen IS (1999) Distribution and prevalence of hyperpolarization-activated cation channel (HCN) mRNA expression in cardiac tissues. *Circ Res* 85:1–6
34. Moosmang S, Stieber J, Zong X, Biel M, Hofmann F, Ludwig A (2001) Cellular expression and functional characterization of four hyperpolarization-activated pacemaker channels in cardiac and neuronal tissues. *Eur J Biochem* 268:1646–1652
35. Marionneau C, Couette B, Liu J, Li H, Mangoni ME, Nargeot J, Lei M, Escande D, Demolombe S (2005) Specific pattern of ionic gene expression associated with pacemaker activity in the mouse heart. *J Physiol* 562:223–234
36. Liu JH, Dobrzynski H, Yanni J, Boyett MR, Lei M (2007) Organisation of the mouse sinoatrial node: structure and expression of HCN channels. *Cardiovasc Res* 73:729–738
37. Maruoka F, Nakashima Y, Takano M, Ono K, Noma A (1994) Cation-dependent gating of the hyperpolarization-activated cation current in the rabbit sino-atrial node cells. *J Physiol* 477:423–435
38. Singh A, Gebhart M, Fritsch R, Sinnegger-Brauns MJ, Poggiani C, Hoda JC, Engel J, Romanin C, Striessnig J, Koschak A (2008) Modulation of voltage- and  $Ca^{2+}$ -dependent gating of  $Ca_v1.3$  L-type calcium channels by alternative splicing of a C-terminal regulatory domain. *J Biol Chem* 283:20733–20744
39. Haase H, Pfitzmaier B, McEnery MW, Morano I (2000) Expression of  $Ca^{2+}$  channel subunits during cardiac ontogeny in

- mice and rats: identification of fetal  $\alpha 1C$  and  $\beta$  subunit isoforms. *J Cell Biochem* 76:695–703
40. Perez-Reyes E (2003) Molecular physiology of low-voltage-activated t-type calcium channels. *Physiol Rev* 83:117–161
  41. Ono K, Iijima T (2005) Pathophysiological significance of T-type  $Ca^{2+}$  channels: properties and functional roles of T-type  $Ca^{2+}$  channels in cardiac pacemaking. *J Pharmacol Sci* 204:197–204
  42. Vassort G, Talavera K, Alvarez JL (2006) Role of T-type  $Ca^{2+}$  channels in the heart. *Cell Calcium* 40:205–220
  43. Ono K, Iijima T (2010) Cardiac T-type  $Ca^{2+}$  channels in the heart. *J Mol Cell Cardiol* 48:65–70
  44. Lee JH, Gomora JC, Cribbs LL, Perez-Reyes E (1999) Nickel block of three cloned T-type calcium channels: low concentrations selectively block  $\alpha 1H$ . *Biophys J* 77:3034–3042
  45. Monteil A, Chemin J, Bourinet E, Mennessier G, Lory P, Nargeot J (2000) Molecular and functional properties of the human  $\alpha 1G$  subunit that forms T-type calcium channels. *J Biol Chem* 275:6090–6100
  46. Mishra SK, Hermsmeyer K (1994) Selective inhibition of T-type  $Ca^{2+}$  channels by Ro 40-5967. *Circ Res* 75:144–148
  47. Liu JH, Bijlenga P, Occhiodoro T, Fischer-lougheed J, Bader CR, Bernheim L (1999) Mibefradil (Ro 40-5967) inhibits several  $Ca^{2+}$  and  $K^+$  currents in human fusion-competent myoblasts. *Br J Pharmacol* 126:245–253
  48. Lei M, Jones SA, Liu J, Lancaster MK, Fung SSM, Dobrzynski H, Camelliti P, Maier SKG, Noble D, Boyett MR (2004) Requirement of neuronal- and cardiac-type sodium channels for murine sinoatrial node pacemaking. *J Physiol* 559:835–848
  49. Janowski E, Cleemann L, Sasse P, Morad M (2006) Diversity of  $Ca^{2+}$  signaling in developing cardiac cells. *Ann NY Acad Sci* 1080:154–164